

E-ISSN: 2664-8784 P-ISSN: 2664-8776 Impact Factor: RJIF 8.26 IJRE 2025; 7(2): 150-157 © 2024 IJRE

www.engineeringpaper.net Received: 21-08-2025 Accepted: 25-09-2025

Kwang Myong Jo
Faculty of Power Engineering,
Kim Chaek University of
Technology, Kyogu 60,
Pyongyang, Democratic

People's Republic of Korea

Myong Guk Won Faculty of Power Engineering, Kim Chaek University of Technology, Kyogu 60, Pyongyang, Democratic People's Republic of Korea

# A new type of differential pulsed eddy current sensor for detecting internal defects in 316 stainless steel materials

# Kwang Myong Jo and Myong Guk Won

**DOI:** <a href="https://www.doi.org/10.33545/26648776.2025.v7.i2b.133">https://www.doi.org/10.33545/26648776.2025.v7.i2b.133</a>

#### **Abstract**

Eddy current technology is widely used as a nondestructive detection technique to detect surface cracks or internal defects of metallic materials. In the past, eddy current technology was used only for defect detection of magnetic materials, but in recent years it has been widely used for defect detection of non-magnetic materials. Since stainless steel is widely used in industry, it is very important to detect the internal defects correctly in various types of stainless steel equipment. In this paper, for detecting internal defects located 6 mm below the surface in a 7 mm thick 316 stainless steel plate, an analytical model of a concentric pulsed eddy current sensor and a differential pulsed eddy current sensor is developed and simulated to compare the sensitivity. Concentric and differential sensors were fabricated and those were experimented with notches on 7 mm thick stainless steel specimens. In concentric sensors, the sensor's detection signal for the defect is too small to detect due to the noise, whereas in differential sensors, much larger signals than noise are detected. The results showed the proposed differential sensor is much superior to the concentric one and is a new type of sensor that can detect defects in the interior of stainless steel material in practice.

Keywords: Pulsed eddy current; differential sensor; analysis model; internal defect; detection signal

#### 1. Introduction

Eddy current technology is a nondestructive testing technique, and its application is increasing day by day. The eddy current technique has the advantages of relatively simple structure, no direct contact with the test specimen, low cost and fast test speed [1]. In eddy current technology, the excitation coil of the sensor is excited at a single frequency or at various frequencies, in order to detect the defects with surface cracks and depth below the surface. The defects below the surface can be detected when high excitation current is added. If a sinusoidal wave is used as the excitation current, an increase in power can cause the excitation coil to become severely heated and damaged, and a higher frequency limits the depth at which the defect can be detected.

The pulsed eddy current (PEC) technique can overcome this limitation. PEC technology is widely used for nondestructive testing of magnetic and nonmagnetic metallic materials [2]. To detect the internal defects of nonmagnetic materials using PEC technology, the control device and sensor must be specially designed.

Xingle Chen detected non-magnetic metal cracks using pulsed eddy current technique [4]. The PEC technique can be used to detect not only the thickness of the metal specimen, but also the stress test [5]. The PEC technique is used to effectively detect surface cracks and defects inside the pipe [6]. The former uses PEC technique to detect defects from the surface in structures with aluminum alloy fixed by a rivet and to evaluate the sensitivity of the sensor under the sensor and the sensor to detect defects in the bottom of the sensor [7]. To increase the detection sensitivity, a differential placement of two sensors is also proposed [8].

Using PEC technique, the hardness of bearing rings can be predicted, cracks and specimen thickness can be quantitatively estimated, subsurface cavities and cracks identified and yield strength evaluated [9]. In addition, some researchers have used magnetic field sensors as receivers of PEC sensors to increase the sensitivity of defect detection [10]. The use of PEC technology has also been investigated to increase the accuracy of detecting non-magnetic internal cracks [11].

Corresponding Author: Kwang Myong Jo Faculty of Power Engineering, Kim Chaek University of Technology, Kyogu 60, Pyongyang, Democratic People's Republic of Korea To detect the deeper defect of nonmagnetic materials using PEC technology, the controller and sensor must be specially designed [12].

When detecting the internal defects of nonmagnetic materials by PEC technology, it is important to increase the excitation power and increase the sensitivity [13]. However, parameters such as pulse amplitude and width cannot be increased beyond the limit. The differential signal of the defective and the defective parts should be obtained to identify the defect.

The main idea in the design of PEC probes is to optimize the magnetic field near the defect to be concentrated to a maximum. The above previous work shows that there are still many problems to be solved in using pulsed eddy current sensors.

In this paper, we have developed a finite element model of a concentric sensor, obtained a relatively sensitive sensor shape, and fabricated the sensor based on it.

In addition, the differential sensor was fabricated in the same way and the comparison experiment with the concentric sensor was carried out. In this paper, the effect of various factors on sensitivity in PEC probes is analyzed using COMSOL Multiphysics 5.4 and the results are examined in detail by experiments. The advantages of the differential sensor are also confirmed through comparative experiments of a new type of differential sensor and a concentric sensor.

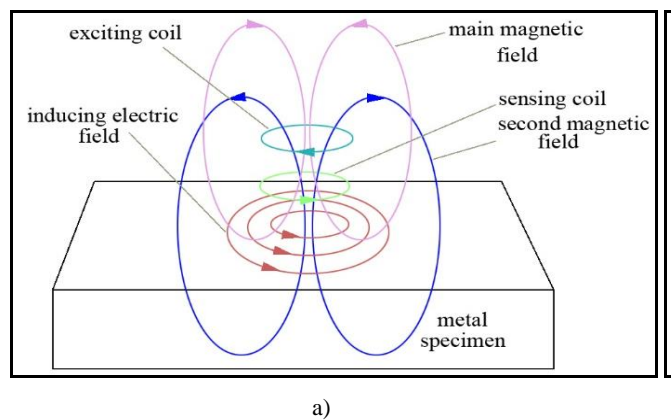
This paper is organized as follows.

In Section 1, the principle of defect detection using eddy currents, and in Section 2, the basic FEM and the research for optimization of probe design are described. Section 3 describes the experimental results and analysis carried out using notches cut on 7 mm thick stainless steel plates.

#### 2. The principle of defect detection using eddy currents

The magnetic field varying according to the electromagnetic induction law generates eddy currents inside the test specimen. This eddy current creates a vortex magnetic field inside the test sample, causing a change in the voltage induced in the sensing coil. This voltage depends on the sensor, theinduharacteristics of the sample, the amplitude and frequency of the excitation current.

The defect detection principle and the equivalent circuit using eddy current are shown in Fig. 1.



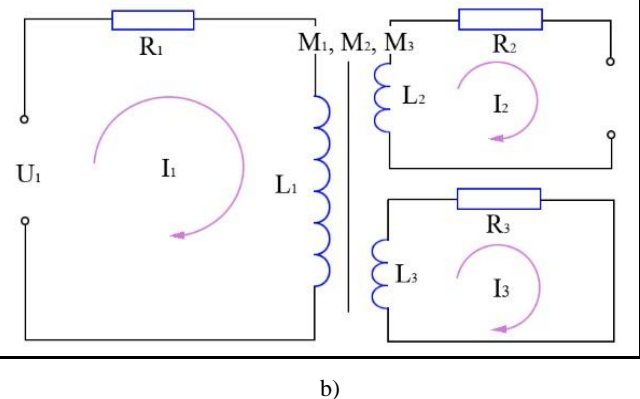


Fig 1: Defect detection principle using eddy current (a) Scheme of defect detection; (b) equivalent circuit.

The mutual inductance between the coil and the sample can be written by Kirchhoff's law as

$$\begin{cases}
R_{1}I_{1} + j\omega L_{1}I_{1} - j\omega M_{1}I_{2} - j\omega M_{3}I_{3} = U_{1} \\
R_{2}I_{2} + j\omega L_{2}I_{2} - j\omega M_{1}I_{1} - j\omega M_{2}I_{3} = U_{2} \\
R_{3}I_{3} + j\omega L_{3}I_{3} - j\omega M_{2}I_{2} - j\omega M_{3}I_{1} = 0
\end{cases}$$
(1)

where R1, L1, I1, U1: resistance of the excitation coil, inductance, current intensity, excitation voltage; R2, L2, I2, U2: resistance of the sensing coil, inductance, current intensity, signal voltage; R3, L3, I3: Resistance of specimen, inductance and current strength; M1, M2, M3: Mutual inductance between sensing coil, excitation coil and specimen.

In Eq.(1), R3, L3, M1, M2 and M3 vary according to the characteristics of the metal specimen (material, structure, defect free state, etc.), and hence the signal voltage U2 is also changed. The eddy current sensor detects defects in metal samples using the relationship between signal voltage U2 and defects in metal samples.

#### 3. Finite element model

## 3.1 Concentric sensor

For finite element modeling of PEC technology, COMSOL Multiphysics 5.4 software was used. In general, the sensing signal from eddy current sensors depends on the magnetic field caused by the excitation current and the change of the magnetic field due to the eddy current generated in the specimen. Here, the magnetic field due to eddy currents varies depending on the structure of the sensor and the characteristics of the specimen. The relationship between magnetic field and signal voltage is shown in Eq. (2).

$$\nabla \times \left(\frac{1}{\mu} \nabla \times \overline{A}\right) = -\sigma \frac{\partial \overline{A}}{\partial t} - \nabla \sigma V + \overline{J}_{s}$$
(2)

where A is the magnetic vector potential VS/m, V is the electric scalar potential V,  $\mu$  is the magnetic permeability H/m,  $\sigma$  is the electric conductivity S/m, and Js is the source current density A/m². We present the following a type of sensor configurations and analyzed the response characteristics using COMSOL Multiphysics 5.4. The model of the sensor is shown in Fig. 2.

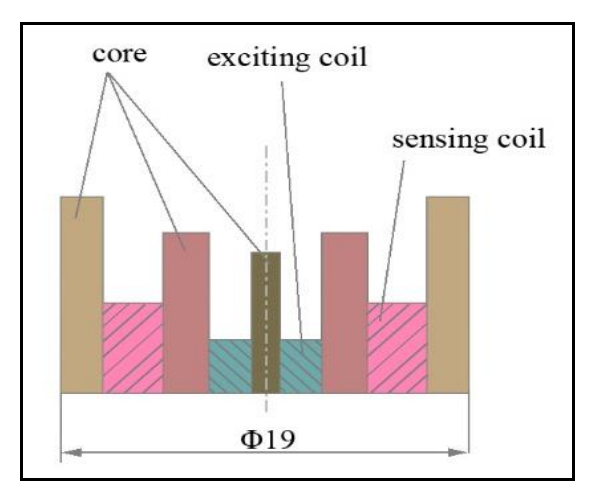


Fig 2: Types of sensors used in the analysis

At that time, the number of turns of excitation and sensing windings is 250 and 1000 turns respectively, and the wire diameter is 0.2mm and 0.05mm. Also, the specimens used in the experiments were 316 stainless steel plates of 240mm, 190 mm and 7mm in length, width and thickness, respectively, and the specimens were artificially fabricated defects 1, 2 and 3. The lengths (75mm) and widths (2mm) of defects 1, 2 and 3 are the same, and the depths are 2mm, 4mm and 6mm, respectively.

The sensor signal in the absence of faults was stored and the real signal was obtained by subtracting this value from the signal in the presence of faults.

Next, the signal intensity was analysed by varying the external diameter of the sensor from 15 to 21 mm to analyze the influence of various factors.

The results are shown in Fig. 3.

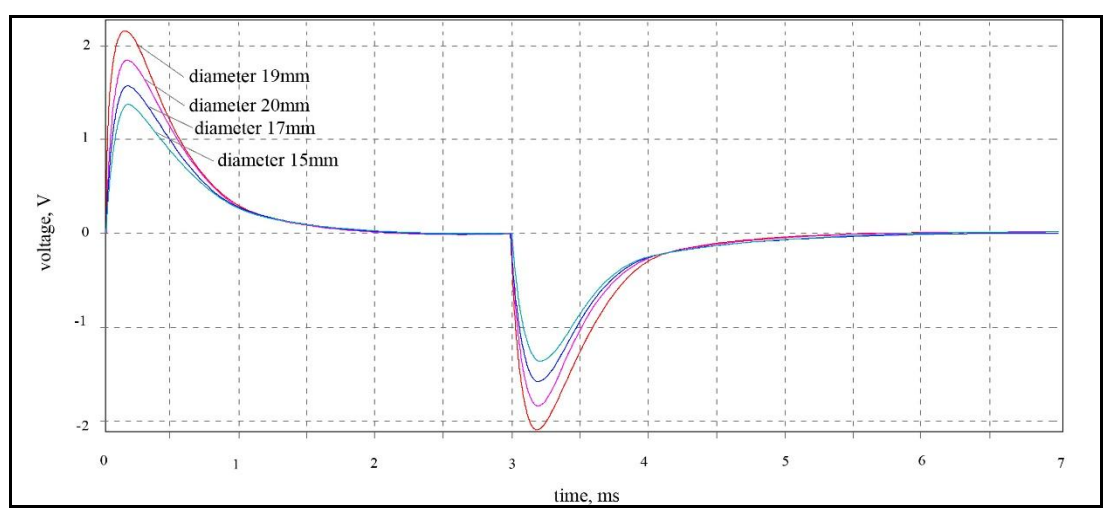


Fig 3: Signal intensity versus sensor outer diameter.

The results show that the signal intensity increases with increasing sensor outer diameter and decreases again at a certain value. This is related to the distribution of the magnetic flux lines, because the eddy current flows more at the defect location when the sensor outer diameter is around 19 mm.

#### 3.2. Differential Sensors

The intensity of the excitation field depends on the intensity of the excitation current, the number of turns of the excitation winding, and the geometry of the winding and the core, and these factors are correlated. Also, the structure of the sensing winding will affect the sensor sensitivity. Thus, the influence of several factors on the sensor output signal must be analyzed accurately to determine the optimum sensor structure and dimensions.

To determine the optimal structure and dimensions of the differential sensor, the influence of various parameters on the sensor output signal was analyzed. For this purpose, the finite element model shown in Fig. 4 was constructed and simulated.

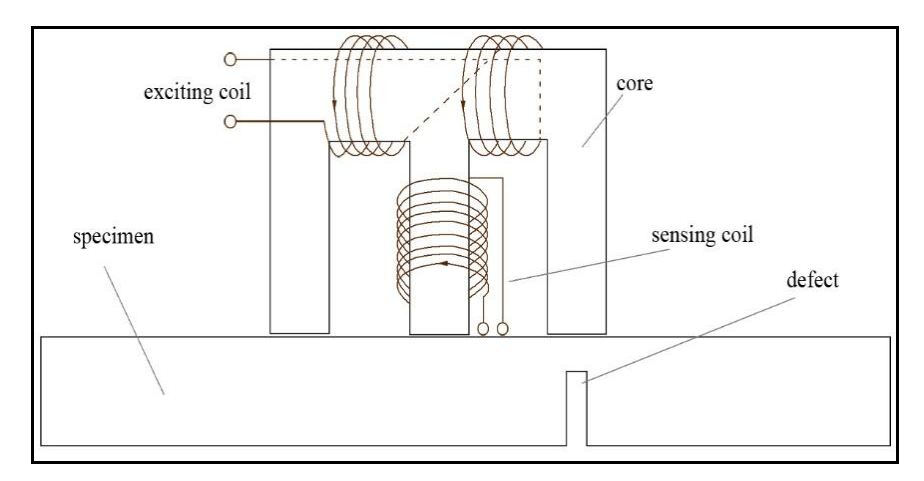


Fig 4: Differential sensor and test specimen model used in the simulation.

The geometry of the E-type sensor and the test specimen used in the simulation are given in Table 1.

**Table 1:** Geometry of the differential sensor and the test specimen with finite element model

Object		Factor	Value
sensor	core	length $L_{\rm c}$ , mm	14
		width $W_c$ , mm	4
		height $H_c$ , mm	7
		$\mathrm{gap}D_{\mathrm{c}}$ , $\mathrm{mm}$	3
	exciting coil	turning number N <sub>e</sub>	100
		coil diameter $D_{\rm e}$ , mm	0.2
	sensing coil	turning number N <sub>s</sub>	200
		coil diameter $D_s$ , mm	0.05
specimen (SS316)	specimen	length $L_p$ , mm	100
		width $W_p$ , mm	40
		height $H_p$ , mm	4
	defect	length $L_{\rm f}$ , mm	20
		width W <sub>f</sub> , mm	0.25
		height $H_{\rm f}$ , mm	2

The model used in the simulation is a three-dimensional model, which selects the simulation mode for magnetic field and electric circuit in AC/DC module and considers the change over time. The boundary conditions were given by natural boundary conditions. The natural boundary condition is the condition under which the magnetic field in the finite element is assumed to act perpendicular to the interface.

For finite element analysis, the model was divided into tetrahedral elements, with a number of elements of 112312. The finite element model used in the calculations is shown in Fig. 5.

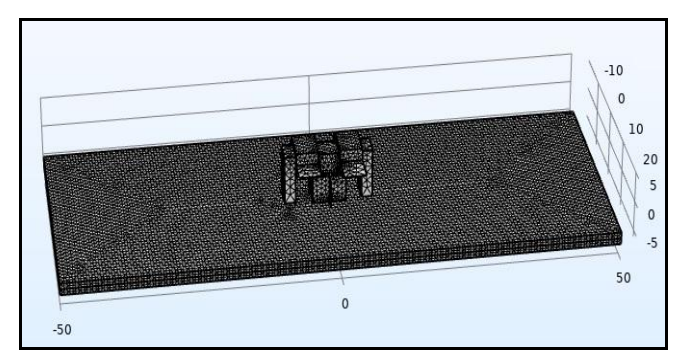


Fig 5: Finite element model used in the calculation.

The external magnetic field of the analytical space was created using an excitation coil. Generally, the allowable current density of copper wire is about 3 A/mm2, and the maximum current that can flow to a 0.2 mm diameter winding is about 0.1A. Hence, the intensity, frequency and duty ratio of the pulsed excitation current were set to 1, 25 and 5%, respectively.

To obtain the output voltage of the sensor according to the defect size and location, the voltage waveforms induced in the sensing winding are considered by varying the value of defect height in the model shown in Fig. 6. The sensor signal voltage waveform along the defect height is shown in Fig. 6.

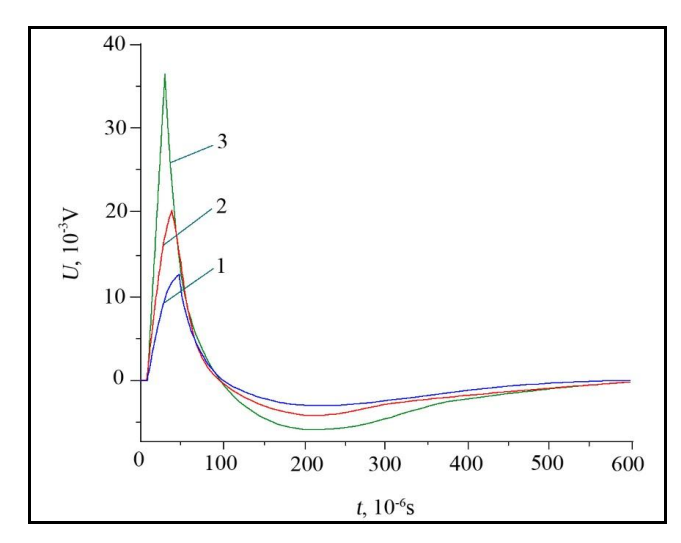


Fig 6: Sensor output signal waveform versus defect height.

1-Defect height 1 mm, 2-Defect height 2 mm, 3-Defect height 3 mm

As can be seen in Fig. 6, the peak amplitude of the signal increases with increasing defect height, and the zero-pass time decreases. This is because the flux through the sensing coil increases as the defect size increases. Thus, the symmetry of the magnetic circuit is destroyed by the defect, which is due to the larger defect size and the stronger the defect size.

Also, as the defect size increases, the effect of eddy currents flowing in the defect becomes stronger, which leads to an increase in the mutual inductance. Thus, the effective resistance component of the winding increases and the reactive resistance component decreases. Because the time constant of the electrical circuit will vary with the magnitude of the fault.

Fig. 7 shows the flux density in the core and the specimen.

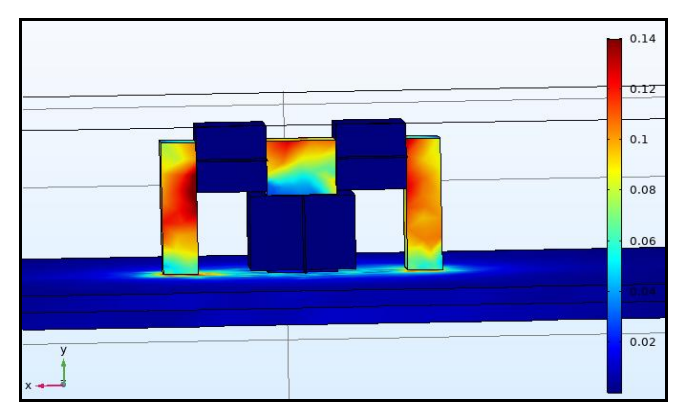
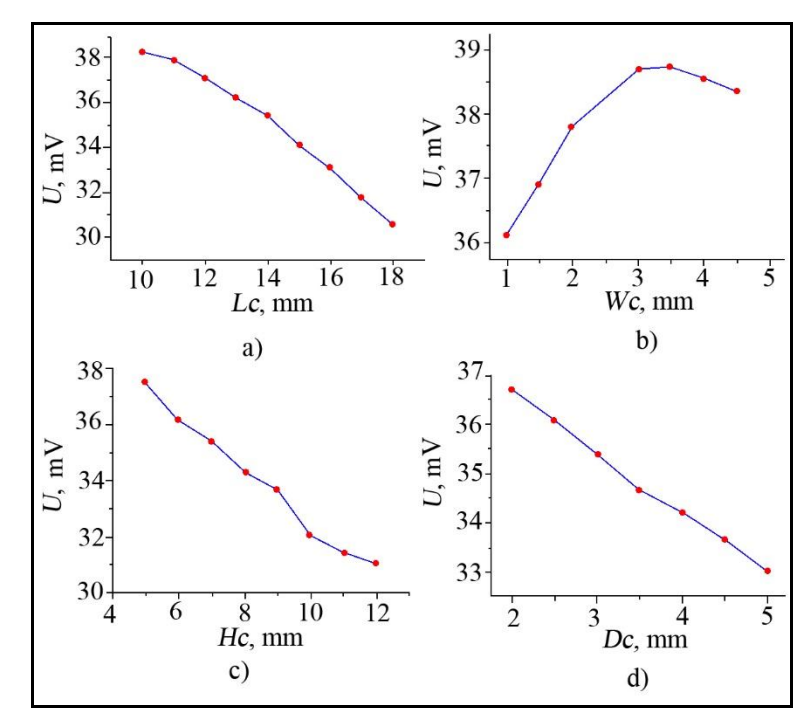


Fig 7: Flux density in the core and specimen.

As can be seen in Fig. 7, the flux density on the left surface of the test specimen is slightly higher than that on the right surface. This is because the reluctance of the right magnetic circuit is large due to the defect. Influence of core dimensions on sensor output signal To investigate the effect of core dimensions on the sensor output signal, Table 1 considers the peak amplitude of the output signal induced by the sensor winding, changing only the core geometry. The results are shown in Fig. 8.



**Fig 8:** Peak amplitude of the sensor output signal versus core dimensions.

a) the effect of length, b) the effect of width, c) the effect of height, and d) the effect of clearance.

As can be seen in Fig. 8a, c, and d, the peak amplitude of the output signal decreases with increasing core length, height and clearance. This is because the magnetoresistance of the magnetic circuit increases with increasing core length, height and clearance.

Also, as can be seen in Fig. 8b, with the increase of the core width, the peak amplitude of the output signal increases and then decreases again when the core width reaches 3 mm. This is because the resistance of the magnetic circuit

decreases with the increase of the core width, but due to the decrease of the flux-line density in the core, the number of flux lines passing through the fault decreases.

To investigate the effect of the number of turns of the excitation and the sensing windings on the sensor output signal, Table 1 considers the peak amplitude of the sensor output signal with varying turns of the excitation and sensing coils.

The results are shown in Fig. 9.

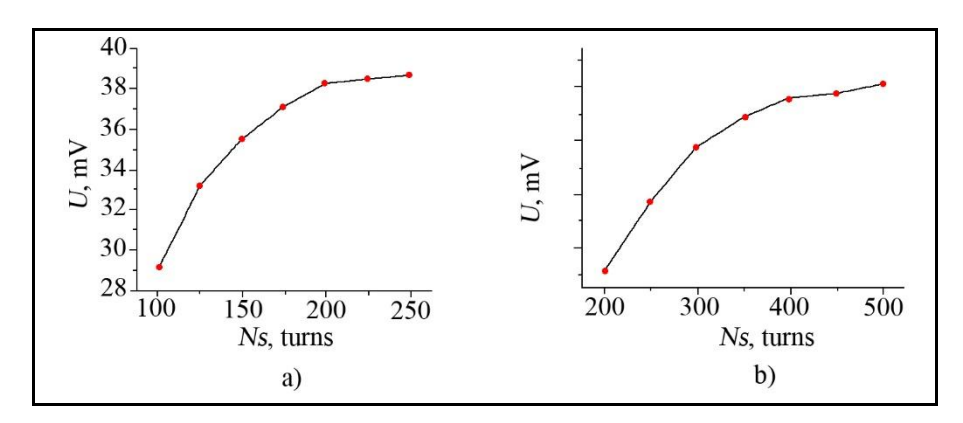


**Fig 9:** Peak amplitude of the sensor output signal versus number of turns. a) Influence of excitation winding turns, b) Influence of sensing winding turns.

As can be seen in Fig. 9a, the peak amplitude of the sensor output signal increases as the number of turns of the excitation winding increases.

However, when the number of turns reaches about 200 turns, the variation is very small. This is because the flux density in the core has almost reached saturation.

As can be seen in Fig. 9b, the peak amplitude of the sensor output signal increases as the number of turns of the sensing winding increases. However, as the number of turns increases, the change becomes weaker. This is because the flux is concentrated in the core. The structure and dimensions of the fabricated sensor are shown in Fig. 10.

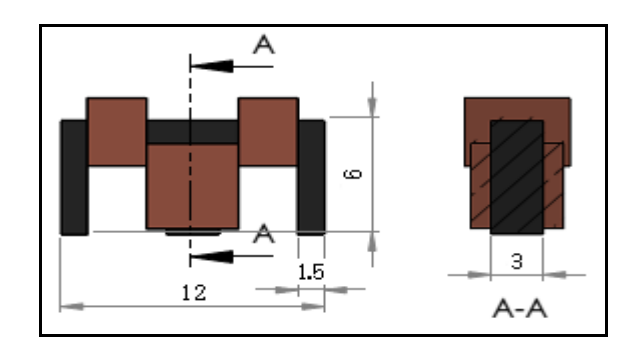


**Fig 10:** Structure and dimensions (in millimeters) of the fabricated E-type sensor.

Here, the diameter and number of turns of the excitation and sensing windings are 0.2 mm, 200, 0.05 mm and 400, respectively.

## 4. Experiments

#### 4.1 Controller and Specimen

The schematic diagram of the fault detection device using pulsed eddy current technique is shown in Fig. 11.

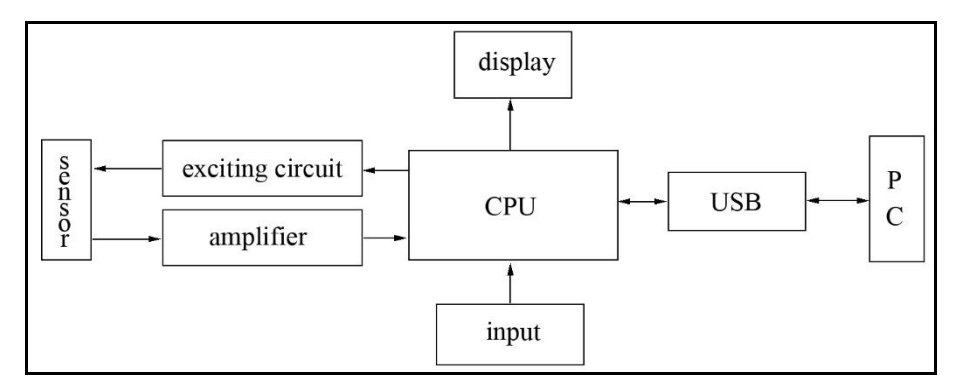


Fig 11: Controller configuration.

The device generates voltage pulses with varying pulse numbers in the range 1-100 pulses/second and pulse widths in the range 0.01-8 ms. In the experiments, an excitation pulse of current 1A, pulse width 3 ms and frequency 20 Hz

was used.

Figure 12 shows the model of edged 316 stainless steel specimens used in the experiments.

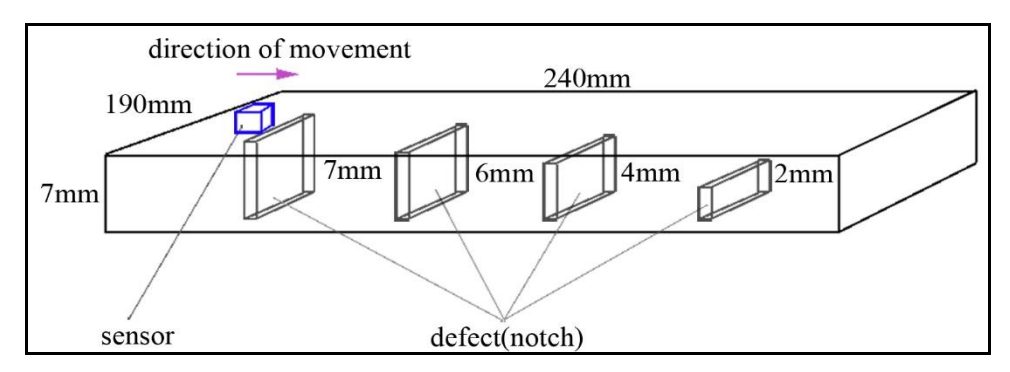


Fig 12: The model of Edged 316 stainless steel specimen.

The specimen is 240 mm  $\times$  190 mm  $\times$ 7 mm (length  $\times$  width  $\times$  thickness) and 4 artificially created defects are present in the specimen. The defects were created using a small-cut

65

65

grinder and a laser-machined machine.

Table 2 gives the geometry and the defect type of the defect formed in the test specimen.

notch

through defect

No	length, mm	whidth, mm	depth, mm	defect type
1	65	2	2	notch
2	65	2	4	notch

Table 2: Geometry and morphology of defects in stainless steel specimens

### 4.2. Experiments on concentric sensor

An image of the concentric sensor is shown in Fig. 13.

4

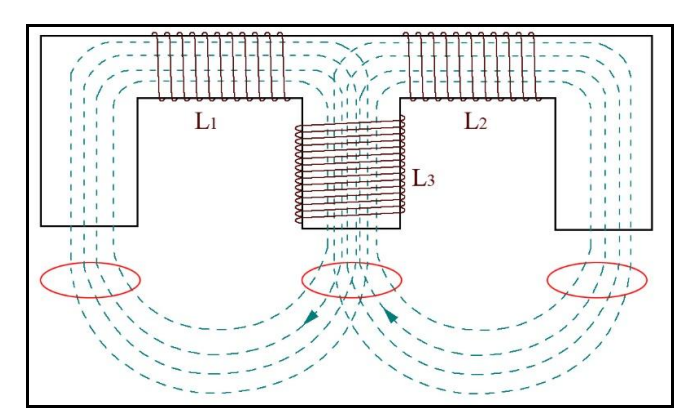


Fig 13: Image of concentric sensor.

The sensor was fabricated by placing a rod core inside the type B used in the finite element model, a sensing coil on top of which was wound 1000 times with 0.05 mm diameter enamel copper wire, and an outer ring with a pump coil on it by 250 turns with 0.35 mm diameter enamel copper wire.

## 4.3. Experiments on differential sensor

Fig. 14 shows the magnetic field distribution of differential sensor.



**Fig 14:** Structure and magnetic field distribution of differential sensor.

As shown in Fig. 14, L1 and L2 are excitation windings and are connected in series in the same direction, so the direction of the magnetic field is the same.

However, in the sensing winding L3, the two magnetic fields cancel out and become zero. For a sample in which the sensor is placed in the atmosphere or without defects, the voltage induced in the sensor winding L3 is zero. The voltage induced in the sensing winding L3 can be considered to depend only on the difference in the magnetic field intensity formed by L1 and L2 and hence only on the eddy currents around the sample below L3.

The number of turns of excitation windings L1 and L2 is 100 turns, the sensing winding is 150 turns, the excitation voltage is 12 V, and the shape of the excitation pulse is the same as in the case of the concentric sensor.

### 5. Results and discussion

#### 5.1 Result

## 5.1.1 Experimental result on concentric sensor

In experiment the gap between the transducer and the sample surface is 0.5mm.

Figure 15 shows the signal waveforms induced in the sensing winding in air.

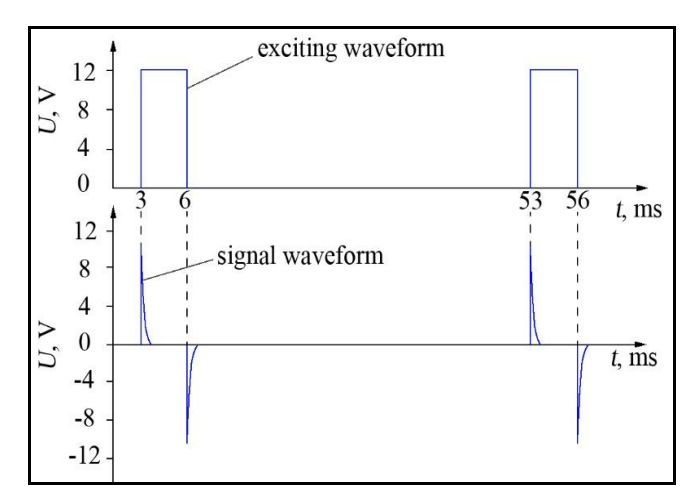


Fig 15: Excitation and signal waveforms.

When the sensor is brought near the sample, the signal waveform changes with distance. The change is significant for the case of the sample magnet, but very little for the case of the non-magnet. Fig. 16 shows the signal waveforms of the sensor for the steel and stainless steel specimens.

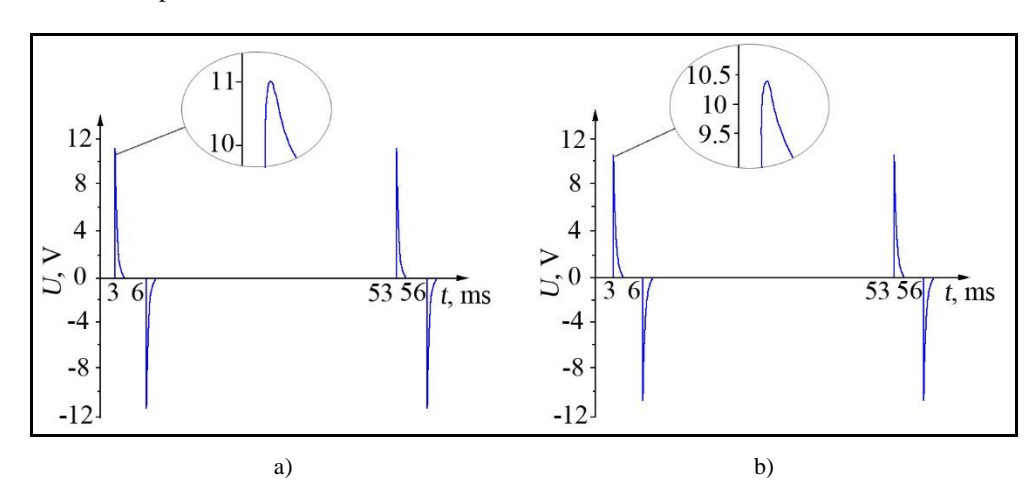


Fig 16: Signal waveforms for steel specimen (a) and stainless steel specimen (b).

The test results for the defects were very difficult to measure for steel specimens, with amplitude variations of 10 mV for the through-through defects and less than 1 mV for the stainless steel specimens. Since the reference signal is as large as 10 V, it cannot be amplified, and therefore, it is difficult to obtain accurate information about the defect. It is possible if the resolution of AD converter is high and various digital signal processing techniques are applied in the computer.

However, further sensitivity of the signal is required to process with a 12-bit AD converter embedded in a chip. The differential sensor is sensitive and zero-reference

The differential sensor is sensitive and zero-reference signal, so there is no such problem. Hence, the experiments were carried out by fabricating a differential sensor.

# 5.1.2 Experimental result on differential sensor

The results of the experiments on the specimens shown in Fig. 13 are shown in Fig. 17.

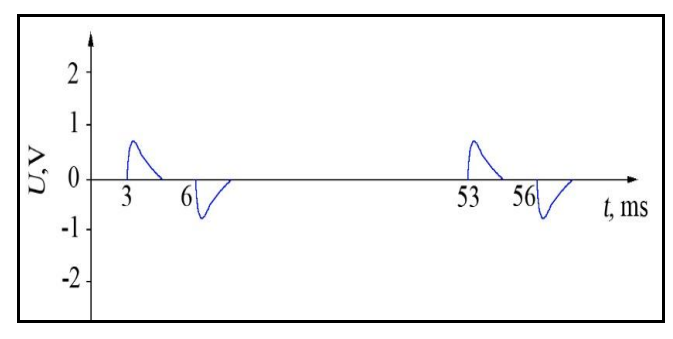


Fig 17: Induced voltage without faults.

In theory, in the absence of faults, the induced voltage must be zero, but small signals are generated due to the structural and material heterogeneity of the sensor core, and the difference in the inductance of the excitation winding. This value does not interfere with the detection of defects because the sample remains constant. The AD convertion rate is 1Msps.

Fig. 18 shows the induced voltage signal with the depth of the defect.

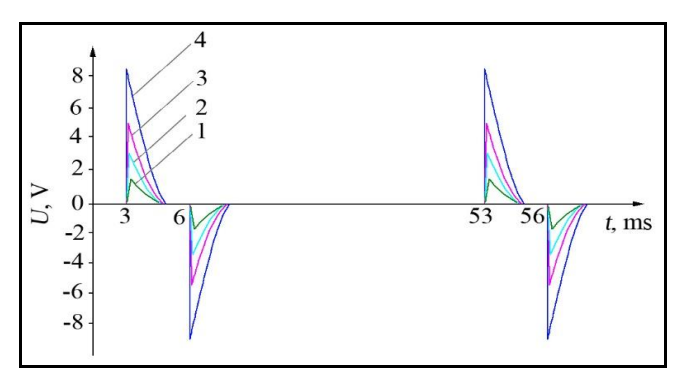


Fig 18: Induced voltage versus depth of defect.

The induced voltages 1, 2, 3 and 4 in Fig. 18 are the result of the measurements in faults 1, 2, 3 and 4 in Fig. 12, respectively. The magnitude of the induced voltage is greatest when one end of the core is placed above the defect. As shown in Fig. 18, the signal of the differential sensor is very large and sufficient to handle without any gain.

# 5.2 Discussion

A relatively high sensitivity configuration for concentric sensors is established through finite element analysis and the sensor is built on the basis of it. The concentric sensor is difficult to measure because the signal strength for defects is very small and strongly influenced by the excitation magnetic field, and the signal processing circuit must be changed whenever the kind of sample changes. However, the differential sensor has a certain rule between the depth of the defect and the signal strength because the signal is zero in the absence of defects and the largest in the case of through defects. It is a very sensitive sensor for measuring surface defects or internal defects, which can be used in practice. The disadvantage is that the defect cannot be measured if it is symmetrically placed on the sensor.

# 6. Conclusions

Through internal defects located 6 mm below the surface in a stainless steel plate of 7 mm thickness, the structural dimensions of the concentric sensor signal are determined and the sensor is manufactured and tested. Concentric sensors can determine the presence or absence of defects, but their size or depth cannot be accurately determined. The differential sensor has been built and tested to have a very high signal strength, a significant change in the depth of the defect, and can be fully processed without amplifying the signal. The study shows differential sensors are effective in detecting internal defects on nonmagnetic objects. The sensor can measure the thickness of the spleen body and align in the circumferential direction, which can be extended in the direction of manufacturing an insert-type and extrapolation-type sensor to detect the defects of stainless steel tube.

#### 7. Acknowledgments

The authors would like to thank Dr. Yong Chan Ri, Myong Guk Pak and Un Hyok Pak for help in analysis and for valuable suggestions and detailed discussions.

#### References

- 1. Hyuga T. Enhance the sensibility of the film infinite eddy current sensors. Journal of International Council on Engineering. 2017;7(1):11-118.
- 2. Chen W, *et al.* Design of a pulsed eddy current testing power supply combining constant amplitude and clamp voltage control. Analog Integrated Circuits and Signal Processing. 2025;122:2-10.
- 3. Zhou D. Optimal features combination for pulsed eddy current NDT. Nondestructive Testing and Evaluation. 2010;25(2):133-143.
- 4. Chen X, *et al.* Pulsed eddy current testing for gap measurement of metal casing. IOP Science. 2022;33(7):1-5.
- 5. Li K. Estimation method of yield strength of ferromagnetic materials based on pulsed eddy current testing. Journal of Magnetism and Magnetic Materials. 2021:1-8.
- 6. Fu Y. Investigation of casing inspection through tubing with pulsed eddy current. Nondestructive Testing and Evaluation. 2012;27(4):353-374.
- 7. Lebrun B, Jayet Y. Pulsed eddy current signal analysis: application to the experimental detection and characterization of deep flaws in highly conductive materials. NDT & E International. 1997;30(3):163-170.
- 8. He Y. Pulsed eddy current technique for defect detection in aircraft riveted structures. NDT & E International. 2010;43:176-181.
- Chen Z. Characterization of image sequences of a defect using pulsed eddy current signals. Journal of Magnetism and Magnetic Materials. 2021;1-11.
- 10. Chen H, Wu X, Xu Z, Kang Y. Pulsed eddy current signal processing method for signal denoising in ferromagnetic plate testing. NDT & E International. 2010;43(7):648-653.
- 11. Wang Z, *et al.* Crack characterization in ferromagnetic steels by pulsed eddy current technique based on GABP neural network model. Journal of Magnetism and Magnetic Materials. 2020;500:1-8.
- 12. Li W. Reconstruction of stress corrosion cracks using signals of pulsed eddy current testing. Nondestructive Testing and Evaluation. 2013;28(2):145-154.
- 13. Shejuan X. Development of a very fast simulator for pulsed eddy current testing signals of local wall thinning. NDT & E International. 2012;51(10):45-50.